DEFLECTION MEASUREMENT THROUGH 3D POINT CLOUD ANALYSIS

by

Bahman Moghaddame-Jafari
A Thesis
Submitted to the
Graduate Faculty
of
George Mason University
in Partial Fulfillment of
The Requirements for the Degree
of
Master of Science
Civil and Infrastructure Engineering

Committee:

__________________________________ Dr. David Lattanzi, Thesis Director

__________________________________ Dr. Girum Urgessa, Committee Member

__________________________________ Dr. Anthony Battistini, Committee Member

__________________________________ Dr. Liza Durant, Department Chair

__________________________________ Dr. Kenneth S. Ball, Dean, Volgenau School of Engineering

Date:______________________________ Fall Semester 2016
George Mason University
Fairfax, VA

Deflection Measurement through 3D Point Cloud Analysis

A Thesis submitted in partial fulfillment of the requirements for the degree of Master of Science at George Mason University

by

Bahman Moghaddame-Jafari
Bachelors of Science
Islamic Azad University

Director: David Lattanzi, Assistant Professor
Department of Civil and Infrastructure Engineering

Fall Semester 2016
George Mason University
Fairfax, VA

DEDICATION

I dedicate my dissertation work to my family and many friends. A special feeling of gratitude to my loving parents, Mohammad-Reza and Soudabeh whose words of encouragement and push for tenacity ring in my ears. My sisters, Bahareh and Beheshteh have never left my side and are very special.

ACKNOWLEDGEMENTS

I wish to thank my committee members who were more than generous with their expertise and precious time. A special thanks to Dr. David Lattanzi, my thesis director for his countless hours of reflecting, reading, encouraging, and most of all patience throughout the entire process. Thank you Dr. Urgessa and Dr. Battistini for agreeing to serve on my committee. I would like to acknowledge and thank the department of CEIE for allowing me to conduct my research and providing any assistance requested. Special thanks goes to LRG research group at GMU in particular, Ali Khaloo for providing technical assistance.

TABLE OF CONTENTS

LIST OF TABLES

LIST OF FIGURES

LIST OF EQUATIONS

LIST OF ABBREVIATIONS

Point Cloud ....PC
Cloud-to-Cloud C2C
Multiscale Model to Model Cloud Comparison M3C2
Point Cloud Data...PCD
Dense Structure-from-Motion ....DSfM
Region of Interest ....ROI

ABSTRACT

DEFLECTION MEASUREMENT THROUGH 3D POINT CLOUD ANALYSIS

Bahman Moghaddame-Jafari, M.S.

George Mason University, 2016

Thesis Director: Dr. David Lattanzi

Point cloud technology is now used in inspection of bridges and tunnels where it is desired to remotely measure the structure’s movements such as settlements and member deformations. Current methods of point cloud analysis for measuring structural deflections require meshing or line/curve fitting to the point cloud data. This step adds an error to the overall accuracy of this technology and is not computationally stable. This study presents a novel method in measuring structural deflections through a per-point sampling method in which the point cloud is directly analyzed without the need for meshing or line/curve fitting. The 3D point cloud data is collected using Photogrammetry and the Structure-from-Motion (SfM) algorithm. The deflections are computed using Cloud-to-Cloud (C2C) distance measurement and Multiscale Model to Model Cloud Comparison (M3C2) algorithms. Through three-point flexural testing, series of aluminum specimens were deflected for validation. Two different statistical methods were used to determine the deflections along the member. The results indicate sub-millimeter accuracy

in measuring vertical deflection. Furthermore, results suggest that this technique can be a tool to update locally the structure’s Finite Element Model to account for deformations in the structure.

CHAPTER 1: INTRODUCTION

Motivation:

Accurate and rapid condition assessment of in-service infrastructure systems is critical for system-wide prioritization decisions. Recently, three-dimensional (3D) scanning has seen expanded use as a modern tool for this purpose. In this context, the results of a 3D scan, referred to as point clouds, can produce highly accurate 3D representations of the in-situ conditions for a given structure that can be leveraged in a variety of ways. The most straightforward approach is to use such 3D scans as a visual record at a given inspection interval. However, it is also possible to computationally compare 3D point cloud reconstructions from consecutive inspection intervals to assess time-dependent phenomena such as changes in boundary conditions or long-term strain effects as theses effects directly affect the load-carrying capacity of the structure. Moreover, in the inspection of bridge clearances, often it is needed to close or restrict the road under the bridge. This could be challenging when the road has high annual daily traffic. 3D scan can be used to inspect and monitor bridge clearances from the side shoulders without the need to restrict or close the road.

There are several methods to generate dense 3D point clouds (Fathi, Dai, and Lourakis 2015). Light Detection And Ranging (LiDAR) is the most common, and a well-established tool in generating point cloud data in the domains of civil surveying and construction, with many commercially available options. However, LiDAR systems can be expensive and susceptible to damage in industrial environments. In addition, these modern remote sensing systems have data collection limitations on sites with limited ground access. An alternative to this approach is to use photogrammetry, the process of taking measurements from images, to generate 3D point clouds. In particular, Dense Structure-from-Motion (DSfM) is capable of producing point clouds with comparable accuracy to those of LiDAR scans while being less expensive (Seitz et al. 2006). The general procedure of 3D reconstruction from 2D images can be broken down into following steps: (i) salient feature point extraction, (ii) robust image matching, (iii) sparse 3D point cloud and (iv) dense point cloud reconstruction. DSfM can also easily be used in conjunction with cameras mounted on unmanned aerial vehicles (UAV) (Lattanzi and Miller 2015).

The point clouds generated using DSfM have the necessary density to capture most of the details of a structure. Therefore, these point clouds could be generated at different instances in time and be compared with a reference point cloud to capture the structural deformations. How accurately these differences can be measured is still unknown and is the motivation for this study.

Purpose of the Research:

The main purpose for this study is to determine the accuracy of deformation measurement through point cloud analysis in structural elements. To achieve this, a sampled-based algorithm was developed. It uses a combination of a direct point-wise distance metric in conjunction with statistical sampling to extract structural deformations. The algorithm was tested on series of laboratory experiments designed to test the proposed approach and the results are presented. As 3D data is becoming more applicable among various industries, specifically Construction and Asset Management, this contribution is introducing a new tool to advance structural inspection documentation as it provides a tool to accurately keep track of any movements in the structure.

Thesis Organization:

The thesis is organized in the following manner. Chapter 2 reviews the related work. The related work in this thesis pertains to the state of the art techniques and computer algorithms in generating and measuring point clouds. Chapter 3 reviews the methods used to generate the point clouds as well as the developed measurement algorithms. Chapter 4 overviews experimental validation procedures including the test apparatus and equipment used to generate the raw data. Also, it presents the results and assessment of each method along with providing a more detailed explanation of the findings. Chapter 5 concludes the study and provides recommendations for advancement and future work.

CHAPTER 2: LITERATURE REVIEW

Point Clouds in Engineering:

3D point cloud techniques have been used in a broad range of inspection and assessment scenarios in various industries. For instance, Gonzalez-Aguilera et al. (González-Aguilera et al. 2013) tested a close-range photogrammetric system to measure vehicles surface areas for condition inspection. The results indicate the values obtained from close-range photogrammetry are clearly better than the conventional method of using measuring tape in terms of time and cost. Baek et al. (Baek, Cho, and Bang 2014) used point clouds in wheel alignment inspection systems for vehicles. A simple and inexpensive method was developed using a consumer-grade depth-sensing camera to get the point cloud data in real-time and conduct the inspection. The experimental results showed that the proposed method provides satisfactory performance. The authors in this study claim that point cloud data has a great potential to be an effective alternative to existing wheel alignment inspection methods. In another case study by Li et al. (Li, Zhou, and Yan 2015) improvements were made in the point cloud-based inspection of blades in aviation, gas, and jet engines.

Point Clouds in Civil Engineering:

Recently, researchers have led an effort to expand the use of these modern remote sensing technologies to broader civil infrastructure applications. Transportation agencies have used 3D modeling as an additional component of Building Information Modeling

(BIM) systems to track the as-built conditions of structures (Pătrăucean et al. 2015). In the case of infrastructure condition assessment, accurately acquiring the geometric information of the structure is a critical parameter. Yilmaturk et al. (Yılmaztürk, Kulur, and Terzi 2010) used close-range digital photogrammetry to measure and monitor deflections in buried flexible pipes. The authors were successful in determining the load-deflection behavior of buried flexible pipes and recognizing this method as a reliable and accurate technique to monitor the pipes in near real time under load conditions. Moreover, Valença et al. (Valença et al. 2013) has developed an automatic monitoring system using photogrammetry and image processing for detecting surface cracks in concrete. The developed method in Valença's research was able to find the pattern and characterize the surface cracks. Chen et al. (Chen, Garbatov, and Soares 2011) investigated the possibility of using photogrammetry to measure weld-induced deformations in a box girder. Cabaleiro et at. (Manuel Cabaleiro et al., n.d.) developed an algorithm to analyze geometric properties of cross-section of timber beams with section loss due to damage. In this study, LiDAR data was used to determine the new section properties of the damaged beam to check the stresses and member capacity. In recent years, significant progress has been made in image-based 3D reconstruction techniques to overcome/lessen the conventional limitations of these algorithms. Khaloo and Lattanzi (Khaloo and Lattanzi 2015) developed the Hierarchical Point Cloud Generation (HPCG) process, designed to generate high-resolution point clouds suitable for structural inspection applications. Their proposed method uses images from different scales and resolutions to generate highly dense and less noisy point clouds capable of resolving 0.1 mm details.

Measuring Structural Deflections in Point Clouds:

A LiDAR system approach was designed and used to measure bridge deflections by Fuchs et al. (Fuchs et al. 2004). The developed method described several applications of high-resolution LiDAR systems, most importantly for deflection measurements during in-service bridge static load testing. Cabaleiro et al. (M. Cabaleiro et al. 2015a) developed an algorithm to measure and model beam deflections from LiDAR-based point cloud data and determine if the deformations were within limits established by structural codes. Several studies have evaluated the accuracy and efficiency of remote sensing techniques, in particular LiDAR, as a potential method for measuring bridge clearance through manipulation of the dense 3D point cloud data (Liu, Chen, and Hasuer 2012; Watson et al. 2011; Bian et al. 2012; Jiang and Jauregui 2010). The study by Jiang and Jauregui used digital close-range photogrammetry to measure deflections in a bridge superstructure. The accuracy of Jiang's method was comparable to that of the conventional surveying equipment (total station) with significantly lower cost and fieldwork. However, the proposed system in Jiang's work has a typical limitation of the photogrammetric techniques, which is camera calibration. The developed method in this work does not require camera calibration and eliminates this typical limitation of photogrammetric techniques. Cabaleiro et al. (M. Cabaleiro et al. 2015b) considered using LiDAR data to develop an automated methodology to measure the torsional and bending deformation in metal beams and also determine the associated stresses within a reasonable error. One of the main limitations of the proposed method was the implementation of polynomial surface fitting to a beam flange prior to deformation analysis, which can result in erroneous measurement in the presence of noise, or if there is missing data in the point cloud.

Research Need and Focus of this Study:

Based on the provided literature review, the idea of using 3D point clouds to measure deformations for inspection and monitoring purposes has been the interest of many fields and industries including structural engineering. However, current methods in point cloud data (PCD) analysis are limited and require the PCD to be meshed or fitted by a line/curve. This step adds an error and reduces the overall accuracy of the technique. In addition, in the current methods the PCDs are not scalable for larger structures. In the prior studies, the PCD is compared against an ideal undeformed shape of an element, which does not directly provide the change between the two inspections intervals. Therefore, there is a need for point cloud measurement method that addresses these limitations.

The focus of this study is to create and test a new analytical method that measures deformations directly from the point cloud data at the resolution level of the raw point cloud without meshing or line/curve fitting, in order to maximize data integrity and minimize the error in sample-based approach. Moreover, the developed technique can directly compare the two point clouds of an element from two different inspection intervals. This provides the ability to directly keep track of deformations from the previous inspections. Furthermore, this study compares the two dominant distance measurements in PCD, the C2C and M3C2 algorithms, and recommends the best practice for structural deflection measurement based on a series of standard laboratory scale flexural experiments.

CHAPTER 3: METHODOLOGY

In this chapter, in order to improve upon the current methods used for PCD comparison, it is first necessary to understand how the raw point cloud data is developed through photogrammetry. Following this discussion, the chapter will present a new point cloud measurement technique, which includes preprocessing, point cloud comparisons, and several tested cloud-sampling approaches to measurement.

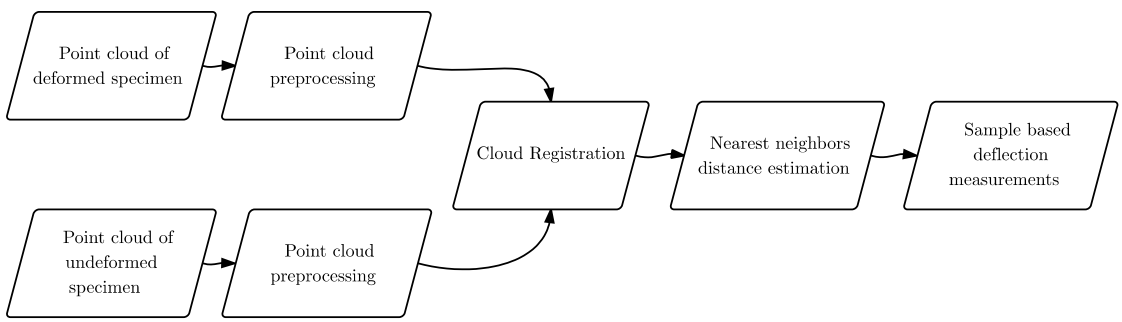

Figure 1. Flowchart of the point cloud measurement process

Figure 1 shows an overall flowchart of the approach. Point clouds of the undeformed and deformed specimens must first be generated for comparison. This way the two point clouds can be superimposed to measure the deflection. The developed approach is applicable for both LiDAR and photogrammetric point cloud generation methods. In this work point clouds were generated using DSfM to validate the proposed cost-effective photogrammetric alternative to LiDAR in generating high-resolution 3D point cloud data using a consumer-grade digital camera.

Point Cloud Generation:

Dense Structure-from-motion (DSfM) (Westoby et al. 2012) is a revolutionary, low-cost, user-friendly photogrammetric technique for obtaining high-resolution point cloud data. DSfM is an automated technique to generate three-dimensional (3D) models of a structure from sequence of two-dimensional stereoscopic images (Figure 2). In contrast with traditional softcopy photogrammetric methods, in which it requires the 3D location and pose of the cameras, the DSfM method solves the camera pose and scene geometry simultaneously using a highly redundant bundle adjustment based on matching features in stereoscopic images. Stereoscopy is a method in which two images of the same object taken at slightly different position are viewed side-by-side to create an impression of depth and solidity. The result is the precise positions of the cameras in space and a dense set of 3D points that includes all fine details of the object of interest.

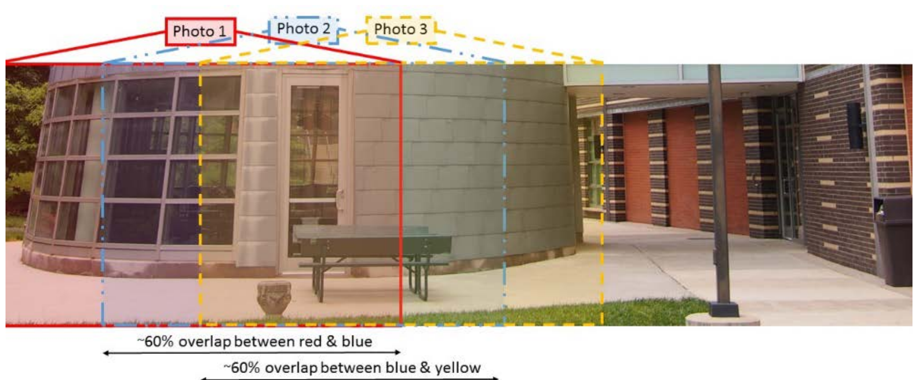

Figure 2, Sequence of two-dimensional stereoscopic images taken for 3D reconstruction using DSfM algorithm

DSfM has many practical applications, yet still is an active research area. Some DSfM applications are still in their early stages of development whereas others are quickly becoming commercially practical techniques in industry, for instance, in 3D Model Reconstruction, 3D Motion Matching, and Robotics. Studies have been done employing different camera specifications, such as wide-lens, fisheye, stereo, catadioptric, pinhole, and multi-camera systems (Mouragnon et al. 2009). Each camera and lens has its own strength and weakness, which directly affects the quality of DSfM results and should be selected relative to the desired outcome.

Point Cloud Pre-processing:

The point clouds are pre-processed to improve the accuracy of the analysis. First, the feature of interest needs to be separated from the rest of the cloud; therefore, extraneous points in the clouds are cropped out. In addition, by applying the statistical outlier removal proposed in (Rusu et al. 2008) unwanted noise in the final 3D reconstructions is detected and removed to minimize point cloud registration failures. The outlier removal module detects these irregularities by computing the mean μ and standard deviation σ of nearest neighbor distances, and trimming the points, which fall outside of $\mu \pm \alpha\sigma$. The value of α depends on the size of the analyzed neighborhood. This also improves computational speed, as the algorithm has fewer points to analyze. Second, the point clouds must be dimensionally scaled using a known distance metric on the structure.

Cloud Registration:

The deformed and undeformed point clouds are then automatically aligned and registered against each other using the Iterative Closest Point (ICP) algorithm (Besl and McKay 1992). The overall aim of the ICP algorithm is to estimate a rigid transformation between $p_i \in P$, a point from the reference 3D point cloud, and $q_i \in Q$, a point from the target point cloud. By using Nearest Neighbors search and Euclidean distance calculation, the algorithm estimates the closest point between p_i and q_i as correspondence points. In order to calculate the rotation R and translation t between p_i and q_i, ICP uses an error function as in Equation 1 to minimize the sum of square distances.

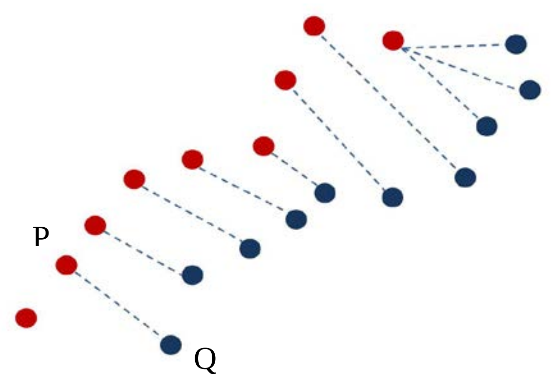

Figure 3. Correspondence estimation between undeformed reference cloud P (red) and deformed cloud Q (blue)

Equation 1. Error function

$$E(R,t) = \min_{R,t} \sum_i \|p_i - (Rq_i + t)\|^2$$

This step can involve partial manual reconstruction; depending on how rough or fine of an alignment is desired. In this experiment, combination of manual and automatic registration is used. Once the two point clouds are spatially registered and scaled, they can then be compared against each other for deformation deviation analysis.

Distance Measurement:

While there are several approaches in literature for direct comparison of 3D points clouds, the two point cloud distance measurement algorithms, Cloud-to-Cloud (C2C) (Girardeau-Montaut et al. 2005a) and Multiscale Model to Model Cloud Compassion (M3C2) (Lague, Brodu, and Leroux 2013), were used to measure the deflections and plot the deformed shapes.

C2C Algorithm:

This method is the simplest direct method in comparing 3D point clouds. It does not require normal calculation or meshing of the data. In this method, for each point of the compared cloud, the algorithm searches the nearest point in the reference cloud and computes their (Euclidean) distance (Figure 4).

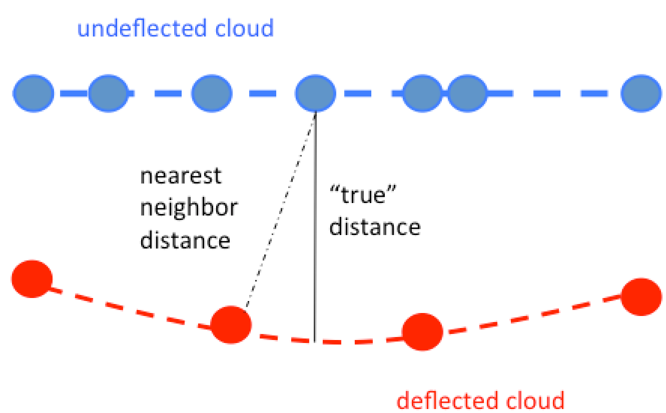

Figure 4. Distance measurement in Nearest Neighbor Search algorithm

Using the undeformed specimen as a reference, the nearest point in the spatially registered cloud of the deformed specimen is estimated and, for instance in C2C algorithm, the Hausdorff distance (Hossain et al. 2011) between the estimated correspondence points is then calculated. Hausdorff distance from set A to set B is a *maxmin* function defines, as

Equation 2. Hausdorff distance

$$H(A,B) = \max_{a \in A}\{\min_{b \in B}\{d(a,b)\}\}$$

where a and b are points of sets A and B respectively, and d(a,b) is any metric between these points. This provides a per-point deflection measurement in the case of beam deformations. These new proposed methods are dependent on the point density variations between 3D datasets, as they do not consider any implicit or explicit surface, but only points. In this study, the generated point clouds had relatively similar local density to minimize inaccuracy in distance measurements. The deformations between the point clouds are rendered as RGB heat maps (Figure 5) for illustrative purposes.

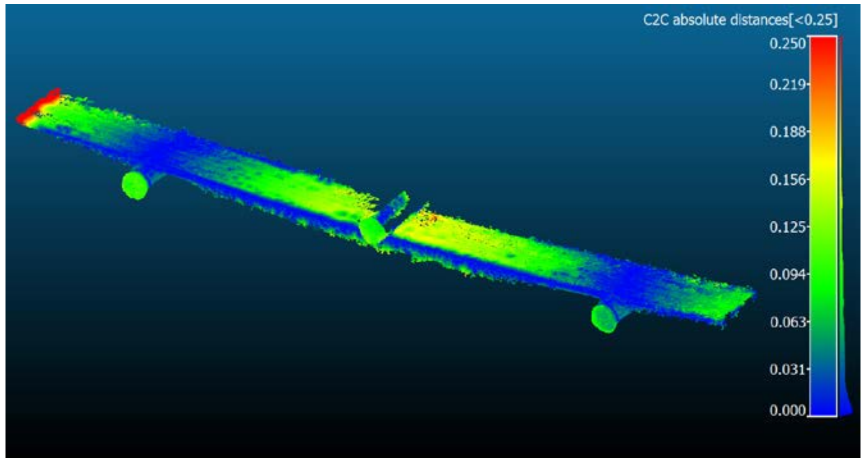

Figure 5. Calculated deflections along the span of the specimen

M3C2 Algorithm:

M3C2 distance calculation is based on set of core points for which distance and confidence interval are calculated. The core points are a sub-sample of the reference point cloud, which can be adjusted by setting minimum point spacing; however, all the calculations are performed on the raw data and only the result is presented on the core points. In M3C2, the normal vector is calculated for each point and sub-clouds that are defined by the intersection of the reference and compared clouds with a cylinder of diameter *d* (projection scale defined by user) and axis (*i*, *N)* (*i* is the core point and *N* is the normal at scale *d*). The intercept of each cloud with the cylinder defines two subsets of points that give two distributions of distances. The mean of the distributions gives the average position of the cloud along the normal direction.

Figure 6 illustrates the two steps of the algorithm: Step 1: In this example, the normal is estimated from cloud 1. In the latter case the scale at which the cloud is the most planar will be selected. Step 2: 2 sub-clouds are defined by the intersection of the reference and compared clouds with a cylinder of diameter d and axis (i, N). Each sub-cloud is projected on the cylinder axis, which gives a distribution of distances along the normal direction. These are used to define the mean (or median) position of each cloud i1 and i2. The local point cloud roughness r1(d) and r2(d) and size n1 and n2 of the 2 sub-clouds are subsequently used to estimate a parametric local confidence interval.

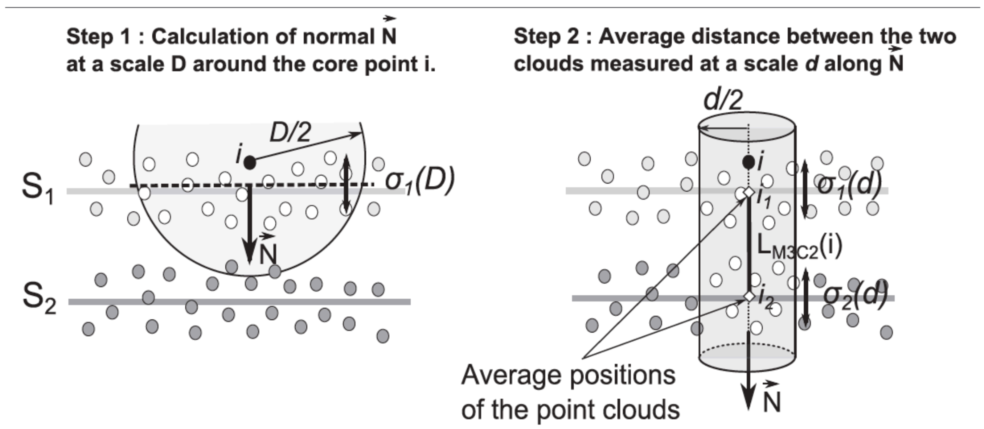

Figure 6. Principle of the Multiscale Model to Model Cloud Comparison (M3C2); (Lague, Brodu, and Leroux 2013)

The results can be shown as a heat map scale, which is the visualization of deformations in the compared point cloud (Figure 5).

This scale may be used when high accuracy is not desired and deformations are large, for instance, deformations that are clearly visible. In addition to low accuracy of using the heat map scale, there were two other issues that needed to be addressed. After running the analysis, each point along the specimen at a given cross section would have a slightly different measurement of deformation. For instance, at quarter span there would be deflections varying ±3 mm. In addition, at midspan the view of the specimen was obstructed due to some part of the testing frame and no data was captured at that region. Therefore, a statistical sampling method was developed to address theses two issues, in addition, to provide basis for an automatic deflection measurement technique.

Region of Interest (ROI):

In order to measure the deflections along the member, the data needed to be subdivided along the member. The point clouds were subdivided into smaller clouds herein referred to as region of interest (ROI). The number and width of each sub-point cloud were determined empirically by analyzing the histogram plots of each ROI. Initially, the histogram of the whole point clouds had multiple peaks, which was not suitable for the proposed sampling technique in this study. Therefore, the point clouds were subdivided to get a histogram at a specific ROI. It was found that the optimum width of each sub-point cloud that would have one peak was 6.35 mm (Figure 7).

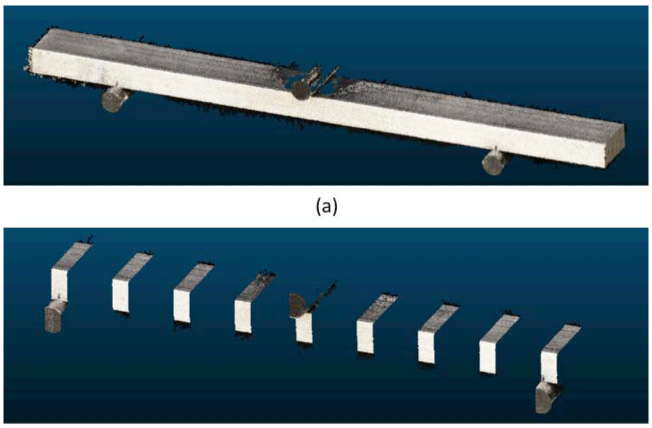

(a)

(b)

Figure 7. (a) Shows the beam before sub-dividing, (b) sub-divided point cloud of the beam

Histograms represent the underlying frequency distribution of a set of data. This allows the inspection of the data for its latent distribution (e.g., normal distribution), outliers, skewness, etc. Moreover, it summarizes large data sets graphically, which is a significant advantage in dealing with point clouds that contains large number of data points. Therefore, histogram analysis of point clouds was used to read the deflection values in each ROI.

Point Sampling:

Two statistical methods were used for deflection measurement in this study, which varies based on the accuracy and level of manual sampling effort. Initially, the 10-point-sampling method was used for the sampling of C2C algorithm only. In this sampling technique, 10 points were selected at the ROI along the beam and the average was calculated to represent the deflection at that location. The second measurement technique involved analysis of the complete set of points at a given ROI. This is due to having multiple peaks in each ROI histogram plot as shown in Figure 8.

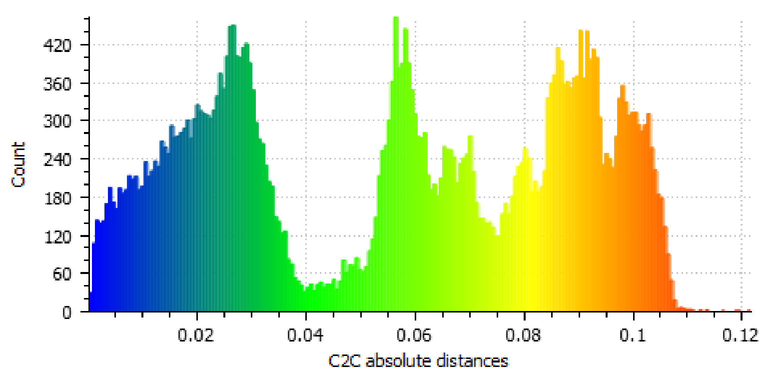

Figure 8. Histogram plot of a ROI after running the C2C distance measurement

Chapter 3 reviewed a photogrammetric technique using DSfM algorithm to generate high-resolution point clouds suitable for monitoring applications and deflection measurement in structural elements. Thereafter, the steps required for preparing the data for distance measurement analysis that are C2C and M3C2 algorithms, are explained. Moreover, the developed sampling technique along with the need and details of creating region of interest in the data is described. In the next chapter, the experiment used to test the developed sampling technique is presented along with the results, findings, and discussions.

CHAPTER 4: EXPERIMENTAL ANALYSIS

Experiment Procedure:

In order to compare the accuracy of the C2C and M3C2 algorithms against conventional methods in measuring structural deflections, a series of flexural tests were designed. All flexural experiments were performed on a Tinius Olsen H50KT Universal Testing Machine (UTM), using a standard three point bending test setup (Figure 9). Aluminum specimens with rectangular cross-sections were tested in order to simplify the measurement and analysis process. Three specimens with different thicknesses were selected to explore the accuracy of the approach at various levels of deflection along with the effects of the object's size in the analysis. The specimens were sequentially loaded up to 75% of the yield capacity, at increments of 10% of the maximum predicted deflection from the theoretical deflection of a simply supported beam.

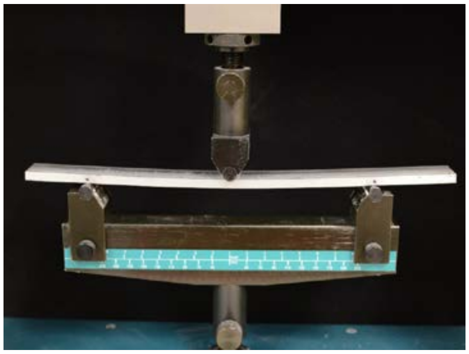

Figure 9. Three point bending test setup

First, point clouds of the undeflected specimens were generated using DSfM. The specimens were then loaded at intervals to cause controlled deflections. At each interval, point clouds of the deformed specimens were generated. Thereafter, the two supports in the three-point bending test were set to be the alignment points for the ICP algorithm as they are fixed with no movement in both stages (deflected and undeflected), enabling high accuracy reconstruction. After registration, each of the deformed point clouds was compared against the reference undeformed point cloud using the presented comparative measurement approach. Since the supports do not deflect in this setup, and at the force point of application (center), the cloud was not as dense due to obstruction in the data acquisition phase. This obstruction was to due to the UTM three-point bending test assembly at the midspan; these segments were excluded from the target set of ROIs (Figure 10).

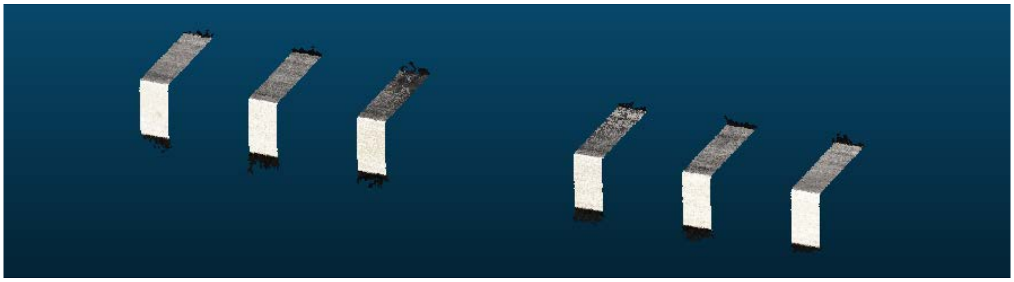

Figure 10. The segments in the cloud selected for analysis

As mentioned earlier, all three specimens were deflected to 75% of their maximum elastic deflection (before yielding; the yielding point is based on the manufacturer's reference) and then the deflection was decreased in set increments (10%

of maximum predicted deflection), seven times, for each specimen. Figure 11 shows each ROI along the specimen. The width of each ROI is 6.35 mm with an average of 44,000 data points per ROI.

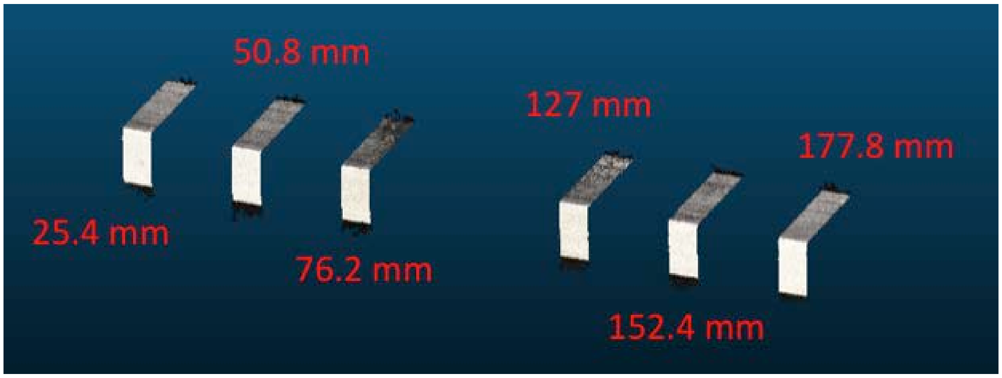

Figure 11. Location of each ROI along the length

The data was imported into MATLAB as text files for the statistical analysis. In each ROI, due to the limitations of the algorithms used for the analysis, only some portion of the points have the true deflection values, this was found by observing the histogram plots of each ROI. Therefore, percentile function was used to subdivide the data within each ROI (sub-point cloud). Figure 10 shows the segmented point cloud. Since the peak in the histogram plot is the deflection at a given ROI and it was observed there are multiple peaks in some ROI histograms, percentile function was used to isolate the one peak that corresponds to the true deflection. The percentile values used to estimate the true deflections were determined empirically. More detail is provided in *ROI Analysis in MATLAB* section.

Specimens:

Table 1 shows the dimensions of the specimens used in this study.

Table 1. Specimen's section properties

Specimen	Length (mm)	Width (mm)	Thickness (mm)	Modulus of Elasticity (GPa)
1	203.2	25.4	3.18	69
2			6.35	
3			12.7	

Camera:

The quality of any DSfM point cloud reconstruction is dependent on: (1) the imaging parameters, (2) the location of the camera for each image, (3) and the number of captured images. The camera model used for this experiment was a Nikon D800E equipped with a Nikon AF-S 50mm or AF-S 105mm lens. The images were taken with sensitivity (ISO) of 400 and the aperture set to *f*/8. A black photo backdrop was placed behind the UTM to help isolate the specimen from the background.

Figure 12. Camera and lenses used for data acquisition

Data Acquisition:

Taking photos from different angles and positions improves the accuracy of the DSfM reconstruction process and results in a more complete, denser and higher quality point cloud. Images were taken in two half-circle movements (Figure 13), first round with the 50mm lens and the second round with the close-up 105mm lens with roughly 70 percent overlap between each image. By varying the focal length of the lens, different levels of detail can be captured and included in the 3D reconstruction. In this study an average of 60 images were taken for each set of point clouds, of which approximately 30 were captured using 50mm lens and the rest with 105mm lens.

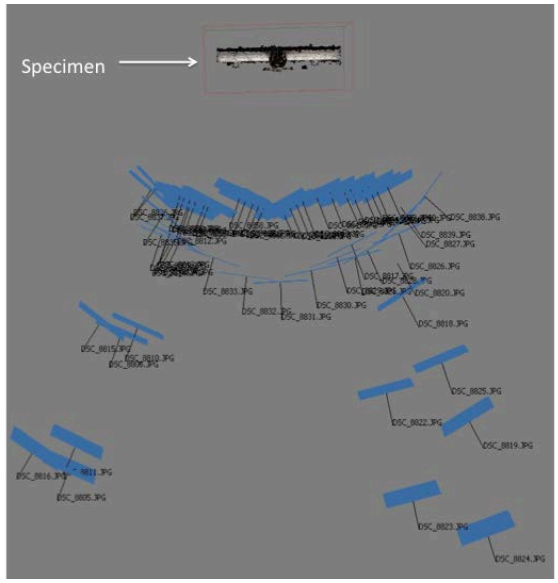

Figure 13. Camera positions during image acquisition, represented as blue rectangles

Computer Programs:

Agisoft PhotoScan (version 0.9.1 2013) was used to create the 3D point clouds. Agisoft employs an adaptation of the Semi-Global Matching algorithm (Hirschmuller 2008) to generate dense reconstructions. In this study, all the images were down sampled by a factor of 2 to efficiently improve computation time and to minimize spurious image features. The dense reconstruction step was performed at "High" quality setting in order to maximize the final point cloud density. Seven point clouds for seven different deflection values were generated for all three specimens (3.18 mm, 6.35 mm, and 12.7 mm), total of twenty-one point clouds (seven from each specimen). Each point cloud is made up of approximately 30,000,000 points with higher density in front and top, and lower density on the back of the specimen and at the point of load application.

Point Cloud Analysis:

There are many computer programs to analyze point cloud data. In this study it was decided to utilize *CloudCompare* (version 2.6.1). Because, it provides various point cloud editing tools (i.e. segmenting, scaling, etc.) and it is open-source.

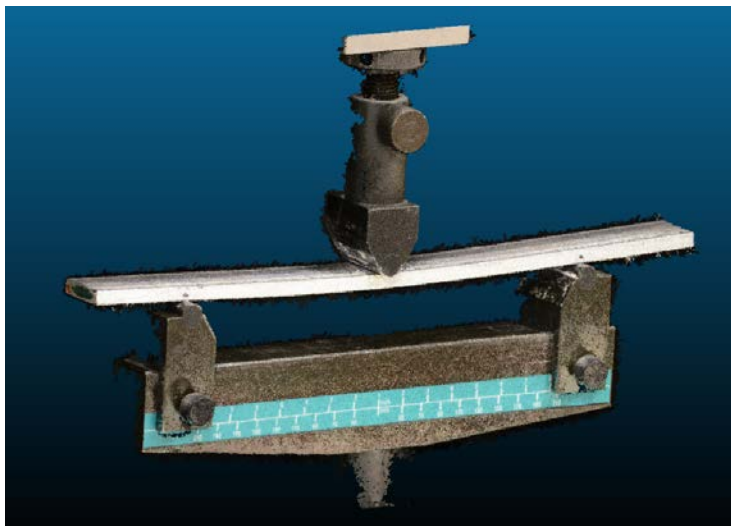

Figure 14. 3D point cloud of a deflected specimen imported to *CloudCompare*

In order to improve the efficiency in the analysis, the excessive parts of the point clouds, for instance the testing frame assemblies, were removed using CloudCompare *segment* tool. After removing the excessive parts, the average number of points in each point cloud was about 14,000,000 points. One undeflected point cloud (no load condition) was generated to serve as a reference for comparison. It was noted that some of the deflected point clouds do not have the same scale as the reference point cloud. Therefore, it was necessary to match the scale of the deflected point cloud to the reference point cloud before running the analysis. In order to accomplish this, the length of the reference specimens was measured and scaled to the real dimension of the specimen, that is 203.2 mm. Then, the length of the unscaled point clouds were measured and divided by the original length to get the scaling factor. Next, by using the *multiply/scale* tool in CloudCompare the unscaled point cloud was multiplied by the factor to get the correct scale. The next step in the process is the alignment and registration of the point clouds. For some of the point clouds, the two clouds coarsely aligned using the "4-Points Congruent Sets for Robust Registration" algorithm (Aiger, Mitra, and Cohen-Or 2008), however, for most of the PCs, fine registration with ICP was used. ICP requires a "model" cloud and a "data" cloud, which in this experiment the undeflected cloud was set to be the "model" cloud. After applying the ICP algorithm to the data, CloudCompare outputs the resulting transformation matrix that was used for final registration. Furthermore, some settings were adjusted in the algorithms before running the analysis to improve the results.

C2C Distance Calculations:

In CloudCompare when this function is called, and after choosing the role of each cloud (reference and data to be compared), a chamfer distance (Butt and Maragos 1998) is automatically computed. After this initial run for approximate distance, the program offers various distance statistics that can refine the distance calculations. These options include:

1. Approximate minimal distance
2. Maximum approximate distance
3. Minimum approximate distance

4. Standard deviation
5. Maximum relative error of the initial approximation
6. Max distance
7. Octree level

Max distance and *Octree level* were specified after initial distance approximation for improving the results. *Max distance* defines a distance above which it is not necessary to calculate a precise distance. This greatly improved the calculations as in this study it was intended to find the smallest deflection; therefore, this parameter was set to a reasonable small distance. Additionally, the *Octree level* parameter significantly improves the results. The *Octree level* is normally optimized automatically by the CloudCompare. The higher the *Octree level*, the more computation is performed on the data. Therefore, only an increment rise in the *Octree level* was used to achieve a better accuracy, yet without a significant increase in computational time. While different *Maximum distances* were used for different clouds, the *Octree level* was set to be constant and equal to eight throughout the analysis.

M3C2 Distance Calculations:

The main difference between M3C2 and C2C is that the computation can only be done on particular point called "core points". The reason for this is to speed up the computations. The idea is since the DSfM-based cloud are generally very dense, it is not necessary to measure the distance at such high density. This is why the operator chooses the feature of interest or core points. The core points can be a sub-sampled version of the input cloud or the whole cloud. It was found that, in this particular experiment, subsampling dramatically reduces the density of the cloud resulting in inadequate data for analysis. Therefore, the whole cloud was set as core points and no reduction in computational speed was used. The *normal scale* is the diameter of the spherical neighborhood extracted around each core point to compute a local normal vector. Although there are advanced options for calculating the normal, this parameter was set to use the normal from the “model” cloud.

ROI Analysis in MATLAB:

MATLAB was used as a platform to run the statistical analysis. The C2C and M3C2 distances for each ROI were saved and loaded into MATLAB as text files. A MATLAB script computed the maximum deflection at ROI based on the classical beam theory. Then, it calculates the deflection in each ROI by using a percentile function. Lastly, it computes the absolute error and plots the deformed shape. Empirically, it was found higher percentiles values (above 80^{th} percentile) yield a smaller absolute error for 3.18 mm and 6.35 mm specimens. In contrast, for 12.7 mm specimen, lower percentile values (below 55^{th} percentile) result in a smaller error. This decrease in percentile can correlate to the slightly higher quality of the thicker specimen’s PCD. Table 2 shows the recommended percentile values for different specimen thicknesses.

Table 2. Recommended percentile values for deflection measurement by means of point cloud analysis

Thickness (mm)	C2C	M3C2
3.18	95	50
6.35	95	50
12.7	50	25

Results:

In this section the results from both non-statistical and statistical methods are presented and compared. Only some of the results are plotted, but all the absolute differences between the PC analysis (C2C and M3C2) and theoretical method are tabulated.

Initial Validation:

Results from initial test indicate that the larger the deformations, the more accurate the algorithms would perform in distance measurement. The results from the 10-point-sampling method (Jafari, Khaloo, and Lattanzi 2016), as well as the validation measurements from the UTM at quarter length of the specimens, are shown in Figure 15 and Table 3. In order to read the measurement at quarter length with the UTM, the applied force was recorded at the midspan and based on that through the simply supported beam deflection equation, the deflection at the quarter length was calculated. The tabular results of C2C algorithm for the 3.18 mm specimen are shown, but the results were similar for the other specimens. For all specimens, the average error was approximately 0.4 mm with variance (S^2) of 0.11, and was consistent between experiments. The results for the 3.18 mm specimen and the 12.7 mm specimen had a higher variance of 0.3 compared to the 6.35 mm specimen.

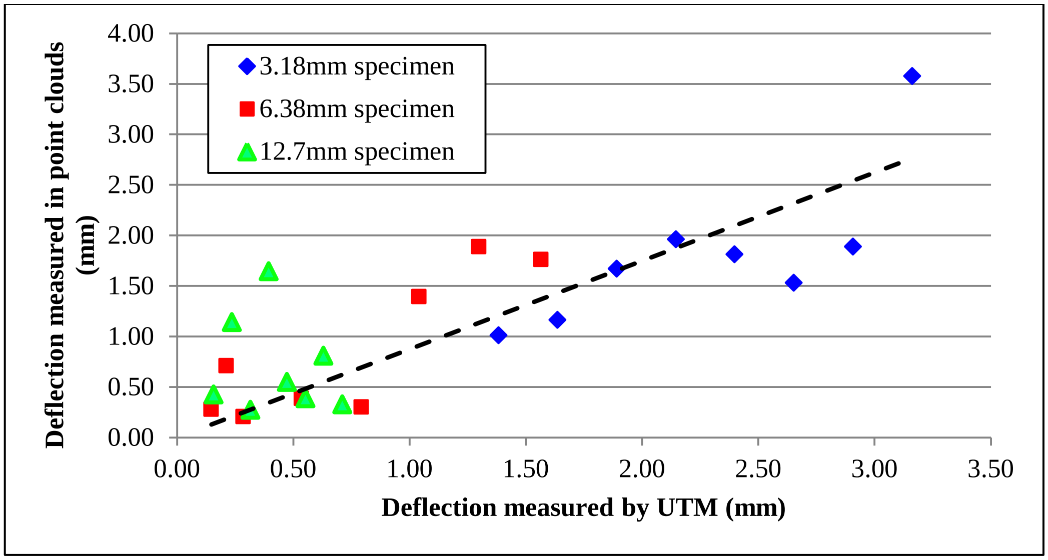

Figure 15. Comparison of UTM and point cloud measurements for all 3 specimens

Table 3. Quarter point measurements for 3.18 mm specimen (the maximum and minimum values are in bold)

UTM (mm)	Point cloud (mm)	Absolute error (mm)
1.38	1.01	0.37
1.64	1.16	0.47
1.89	1.67	0.22
2.15	1.96	**0.19**
2.4	1.81	0.59
2.65	1.53	**1.12**
2.91	1.89	1.02
3.16	3.58	0.41

C2C Results:

Figure 16 shows the deflection values obtained from C2C algorithm compared with theoretical values for the 3.18 mm specimen at the 95th percentile.

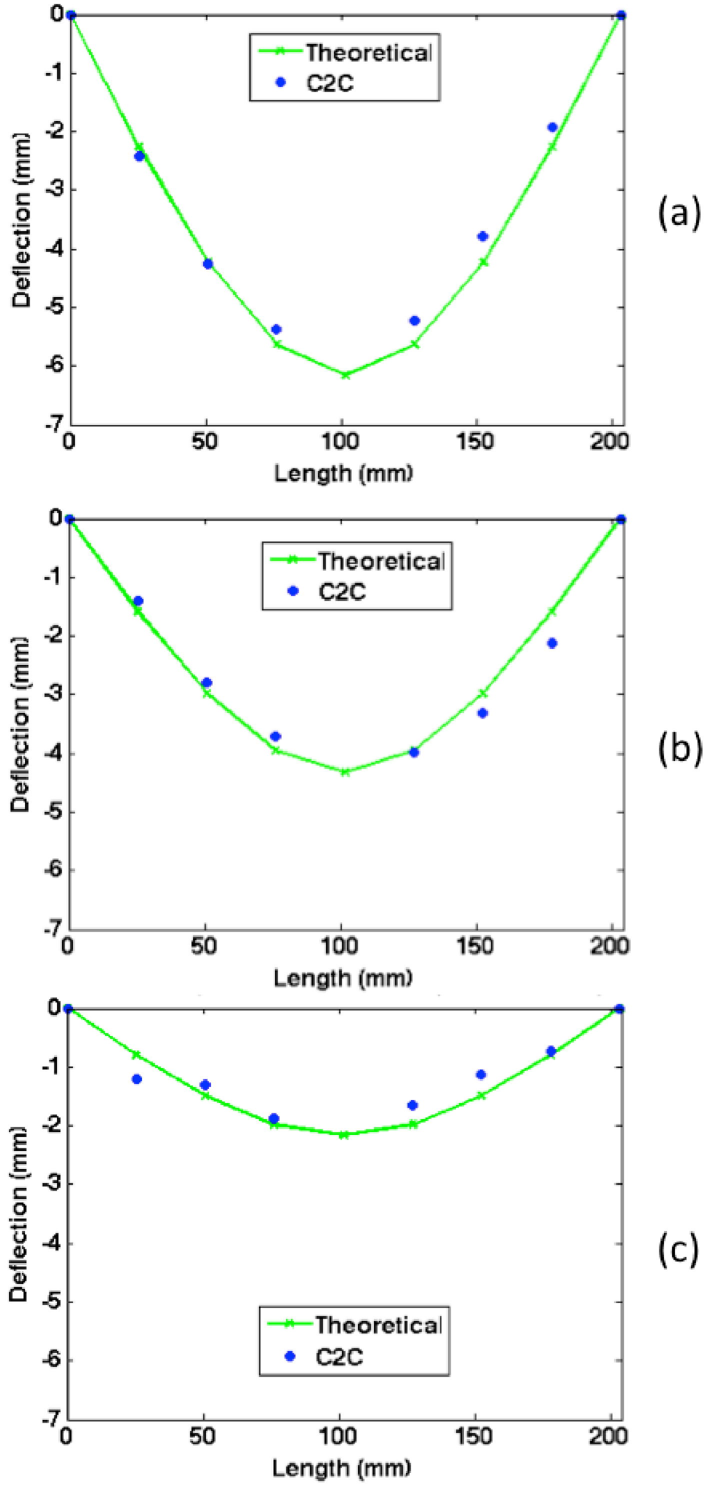

Figure 16. C2C deflection measurements at three deflection levels for the 3.18 mm specimen

In general, as Figure 16 shows, as the deflections get smaller, the absolute error increases. In Figure 16 (a) at the theoretical deflection of 6.3 mm (maximum deflection in this experiment), the developed sampling method measured the deflections at ROIs with the absolute error of 0.26 mm, which is smaller than the average error of 0.4 mm for this specimen for the C2C algorithm. Figure 16 (b) shows the measurements on the left side of the specimen are lower than the right side of the specimen; this indicates ICP registration error. This error indicates that the alignment points (supports) in the deflected point cloud were not adequately positioned on the alignment points of undeflected point cloud. In Figure 16 (c), at midspan deflection of 2.3 mm, the sampling method was not as successful in capturing the deflection at the first ROI (x=25.4 mm). While this was only the case for this particular point cloud and not the rest of the data, it seems there was noise in that ROI at the point cloud generation step.

Figure 17 shows the same deflection calculations at three deflection levels for the 6.35 mm specimen.

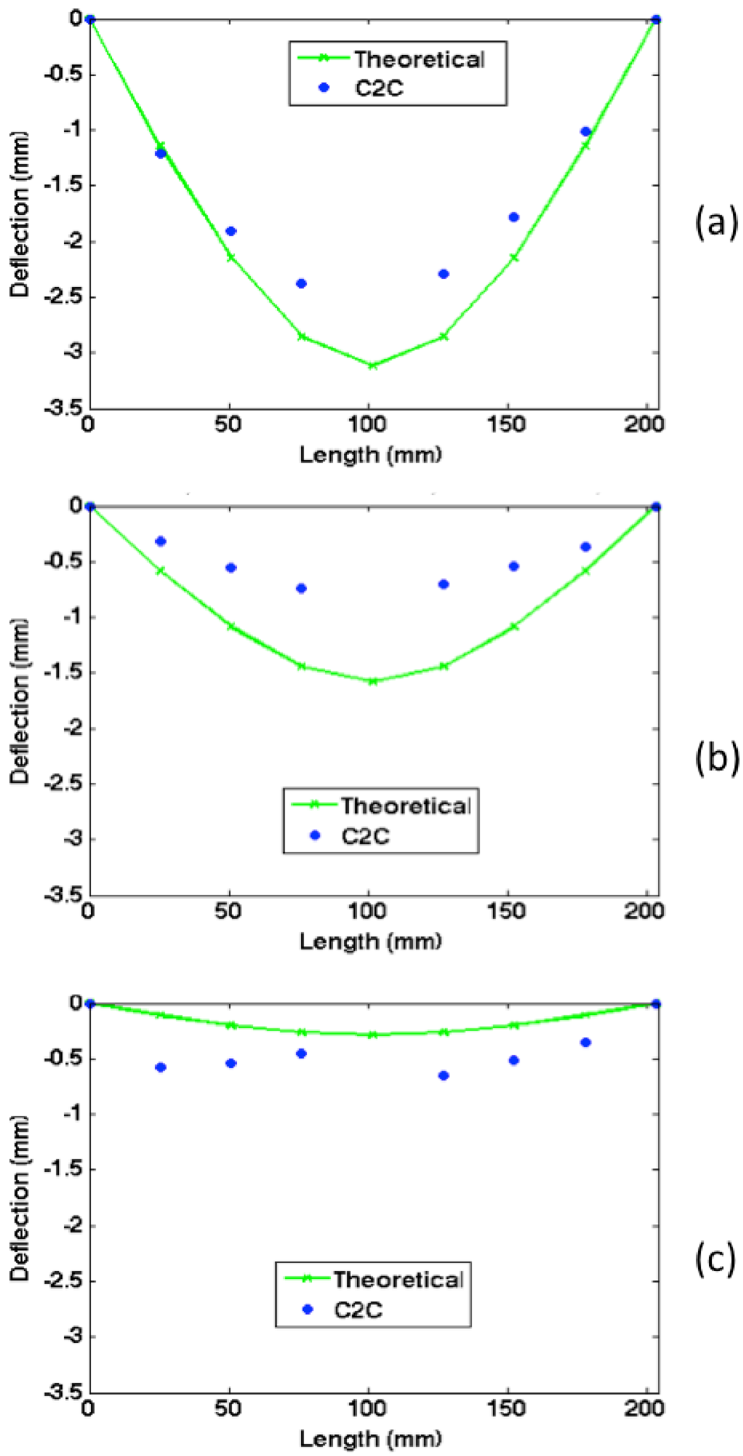

Figure 17. C2C deflection measurements at three deflection levels for the 6.35 mm specimen

In Figure 17 (a), the sampling method was able to estimate the deflection and determine the deformed shape of the specimen. Registration error does not appear to be an issue here. Figure 17 (b) shows the deformed shape, yet with a slightly higher measurement error. This slight increase in error could be due to another ICP registration form of error, that is, the deflected point cloud at the registration phase was slightly above the undeflected point cloud in the vertical direction. In Figure 17 (c), the method was able to estimate the deformations in ROI with an error of 0.27 mm, smaller than the average error of 0.37 mm for this specimen for the C2C algorithm. However, the technique could not estimate the deformed shape. It seems that the midspan deflection (0.3 mm) is in the range of the noise floor of the point clouds and the algorithm could not perform well.

Similarly, Figure 18 shows the Cloud-to-Cloud (C2C) distance measurement at three deflections for 12.7 mm specimen.

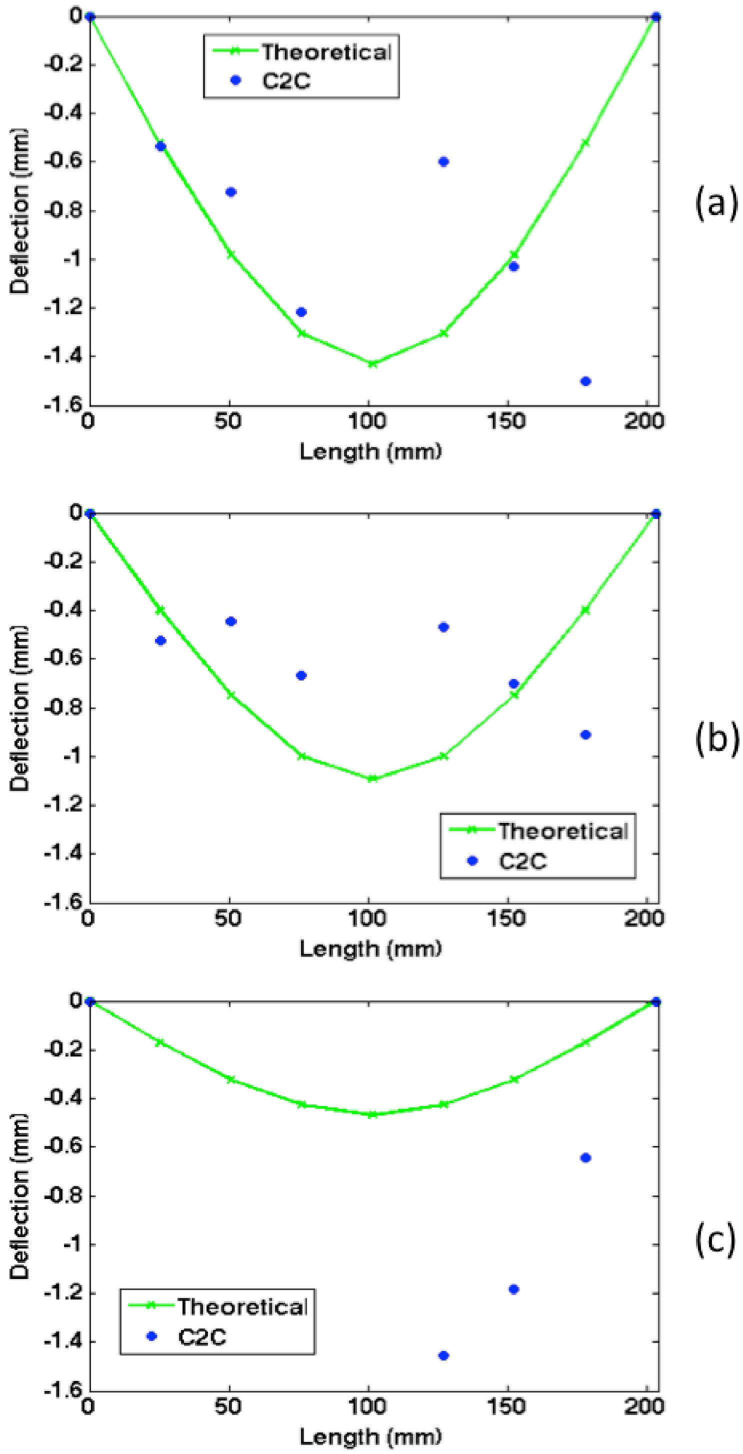

Figure 18. C2C deflection measurements at three deflection levels for the 12.7 mm specimen

As it seems in Figure 18, the sampling method was able to capture the deflections with an average error of 0.9 mm (Table 6); however, the sampling technique could not estimate the deformed shapes. This is due to small deflections (under 2 mm) that seem to be in the noise floor rage of the data for C2C. Moreover, the percentile is decreased to 50. This decrease in percentile is due to having better data quality. Therefore, increase in thickness, improved the quality of the point cloud data and consequently, the distance measurement. Table 4 through Table 6 show the absolute error for all seven deflections with respect to theoretical values (max and min values are bolded).

Table 4. C2C absolute error for the 3.18 mm specimen; mean=0.4; standard deviation=0.28

	Absolute Errors (Locations Along the Specimen (mm))					
Deflections (mm)	**25.4**	**50.8**	**76.2**	**127**	**152.4**	**177.8**
6.33	0.16	**0.02**	0.26	0.40	0.44	0.33
5.82	0.11	0.08	0.70	**1.08**	0.49	0.10
5.31	0.98	0.85	0.65	0.47	0.30	0.24
4.80	0.56	0.44	0.21	0.48	0.71	**1.08**
4.30	0.19	0.18	0.24	0.03	0.33	0.53
3.78	0.07	0.17	0.09	0.35	0.63	0.94
2.77	0.15	0.31	0.53	0.49	0.38	0.13

Table 5. C2C absolute error for the 6.35 mm specimen; mean=0.37; standard deviation=0.24

	Absolute Errors (Locations Along the Specimen (mm))					
Deflections (mm)	**25.4**	**50.8**	**76.2**	**127**	**152.4**	**177.8**
3.11	0.06	0.24	0.48	0.56	0.37	0.13
2.60	**1.07**	0.71	0.39	0.14	0.58	0.92
2.09	**0.02**	**0.02**	0.06	0.31	0.49	0.33
1.58	0.26	0.54	0.71	0.75	0.55	0.22
1.07	0.42	0.20	0.13	0.28	0.39	0.67
0.57	0.53	0.17	0.09	**0.02**	0.39	0.45
0.29	0.47	0.34	0.18	0.38	0.31	0.25

Table 6. C2C absolute error for the 12.7 mm specimen; mean=0.9; standard deviation=0.73

	Absolute Errors (Locations Along the Specimen (mm))					
Deflections (mm)	**25.4**	**50.8**	**76.2**	**127**	**152.4**	**177.8**
1.42	**0.01**	0.26	0.09	0.71	0.04	0.98
1.26	0.78	0.28	**0.01**	0.17	0.58	1.31
1.11	1.12	0.08	0.58	0.07	0.15	0.70
0.95	**2.46**	1.63	1.75	2.02	1.84	2.14
0.79	1.71	1.73	1.42	1.20	1.60	1.99
0.63	0.33	0.34	0.28	0.34	0.33	0.34
0.47	2.13	1.66	1.23	1.03	0.86	0.47

In summary, C2C algorithm was capable of measuring the vertical deflections with mean absolute error of 0.57 mm and mean standard deviation of 0.42 for all three specimens.

M3C2 Results:

Figure 19 shows the M3C2 deflection measurement at three different deflection levels for the 3.18 mm specimen.

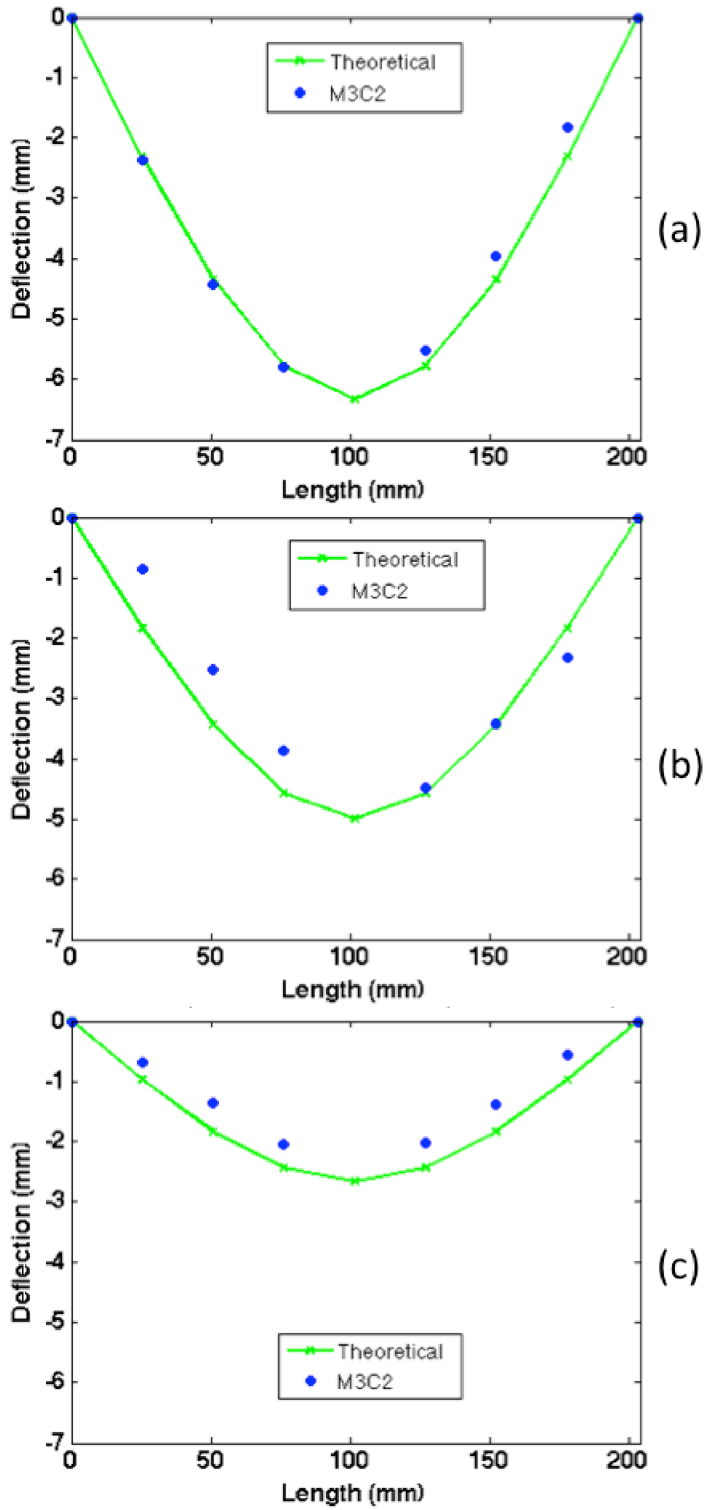

Figure 19. M3C2 deflection measurements at three deflection levels for the 3.18 mm specimen

The overall percentile values is decreased to 50, which indicates that 50% of the data is adequate for distance measurements whereas with C2C algorithm it is 95^{th} percentile for 3.18 mm and 6.35 mm specimens. Figure 20 shows the results for 6.35 mm specimen.

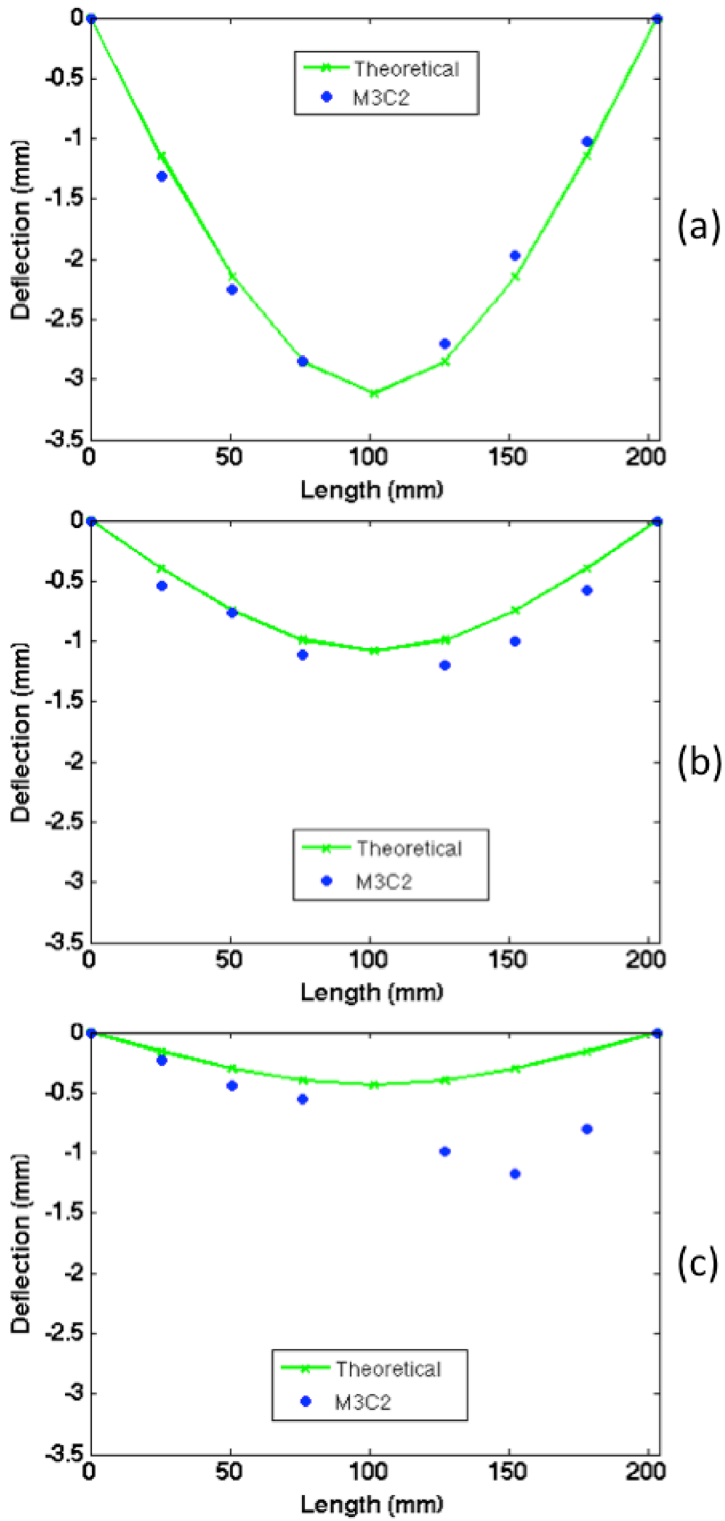

Figure 20. M3C2 deflection measurements at three deflection levels for the 6.35 mm specimen

Figure 20 (c) shows the sampling method cloud not estimate the deformed shape for deflections under 0.4 mm; however, the absolute errors are still acceptable.

Figure 21 shows the M3C2 results for the 12.7 mm specimen. As a reminder, the percentile value for 12.7 mm was decreased to 25th due to the higher thickness.

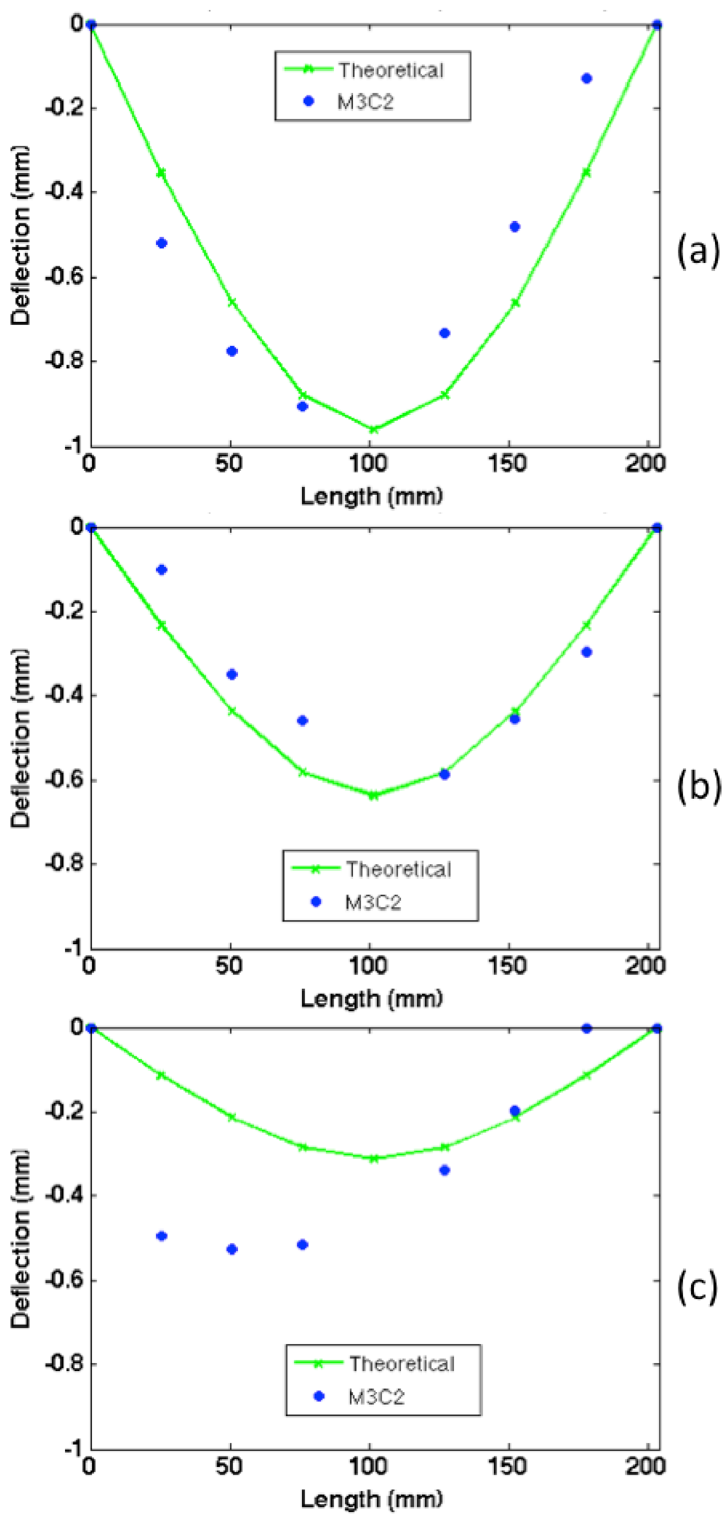

Figure 21. M3C2 deflection measurements at three deflection levels for the 12.7 mm specimen

Figure 21 (a) and (b) show possible registration error, as the measurements are lower on one side and higher on the other side. This means that in small deflection, data sampling is more sensitive to registration and requires more attention.

In Figure 21 (c), even though the deflections are estimated within a reasonable error at each ROI, the deformed shape is not estimated. Most likely this is due to the range of noise floor in the PCD for M3C2, which seems to be at 0.3 mm.

The M3C2 results show that the increase in thickness would decrease the percentile value. This means more data points are equal to the true deflection within each ROI. The larger the specimen, the more data points it will have, thus it can perform better in estimating the deflection. Using more lenses with larger focal lengths may have improved the quality of thinner specimens, but the tradeoff is higher cost and time for data acquisition process. Figure 22 shows the same deflection of 0.6 mm for the 6.35 mm and 12.7 mm specimens.

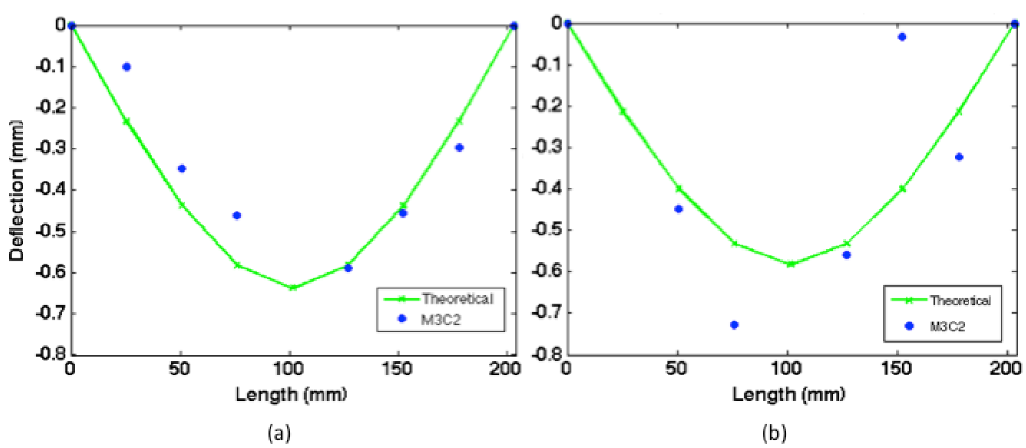

Figure 22. Effects of thickness in M3C2 deflection measurement; (a) 12.7 mm, (b) 6.35 mm; midspan deflection 0.6 mm

The thicker specimen's point cloud provided better data to capture the deformed shape as well as the deflection. This is due to the higher density of the thicker specimen's point cloud.

Table 7 through Table 9 show the absolute differences for all three specimens at the seven deflections considered in the analysis (max and min values are bolded).

Table 7. M3C2 absolute error for the 3.18 mm specimen; mean=0.41; standard deviation=0.51

	Absolute Errors (Locations Along the Specimen (mm))					
Deflections (mm)	**25.4**	**50.8**	**76.2**	**127**	**152.4**	**177.8**
0.25	0.06	0.07	0.02	0.25	0.39	0.49
0.23	1.29	**3.35**	3.01	2.84	3.29	1.00
0.21	0.56	0.65	0.76	0.70	0.81	0.90
0.19	0.98	0.91	0.71	0.08	**0.01**	0.49
0.17	0.34	0.30	0.26	0.10	0.20	0.26
0.15	0.27	0.30	0.24	0.26	0.48	0.72
0.13	0.06	1.68	2.25	2.31	1.78	0.50

Table 8. M3C2 absolute error for the 6.35 mm specimen; mean=0.29; standard deviation=0.27

	Absolute Errors (Locations Along the Specimen (mm))					
Deflections (mm)	**25.4**	**50.8**	**76.2**	**127**	**152.4**	**177.8**
0.12	0.16	0.10	**0.00**	0.15	0.17	0.12
0.10	0.90	0.94	0.77	0.70	0.94	1.13
0.08	0.29	0.32	0.96	0.12	0.10	0.24
0.06	**0.00**	0.97	**1.20**	1.06	0.92	0.01
0.04	0.14	0.02	0.13	0.21	0.26	0.17
0.02	0.08	0.05	0.20	0.03	0.37	0.11
0.018	0.25	0.32	0.35	0.81	1.04	0.84

Table 9. M3C2 absolute error for the 12.7 mm specimen; mean=0.5; standard deviation=0.48

	Absolute Errors (Locations Along the Specimen (mm))					
Deflections (mm)	**25.4**	**50.8**	**76.2**	**127**	**152.4**	**177.8**
0.06	0.40	0.97	1.17	0.90	0.04	1.13
0.05	0.50	0.08	0.71	0.19	0.83	1.65
0.04	0.37	0.68	0.77	0.92	0.18	0.68
0.04	0.12	**0.02**	0.08	0.21	0.25	0.31
0.03	1.97	1.72	1.22	0.99	1.95	**2.52**
0.02	0.18	0.14	0.15	0.07	0.03	**0.02**
0.018	1.06	0.92	0.71	0.52	0.42	0.29

The absolute error distribution presented in the next section show the M3C2 algorithm performed better in detecting the similar points in point clouds resulting in a more accurate distance measurement with the mean absolute error of 0.4 mm and average standard deviation of 0.42.

C2C vs. M3C2:

The histogram plots of absolute errors indicate that the average errors of 0.57 mm and 0.4 mm for C2C and M3C2 respectively. These two error values are the average for the all three specimens.

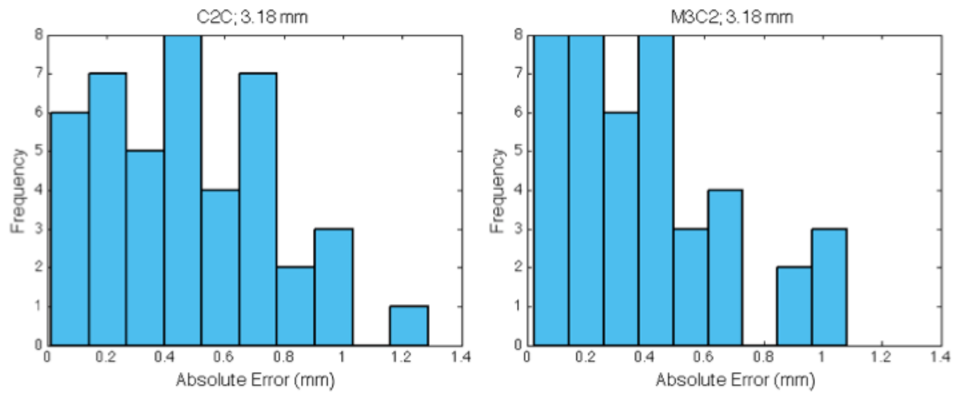

Figure 23. Absolute error distribution of 3.18 mm specimen

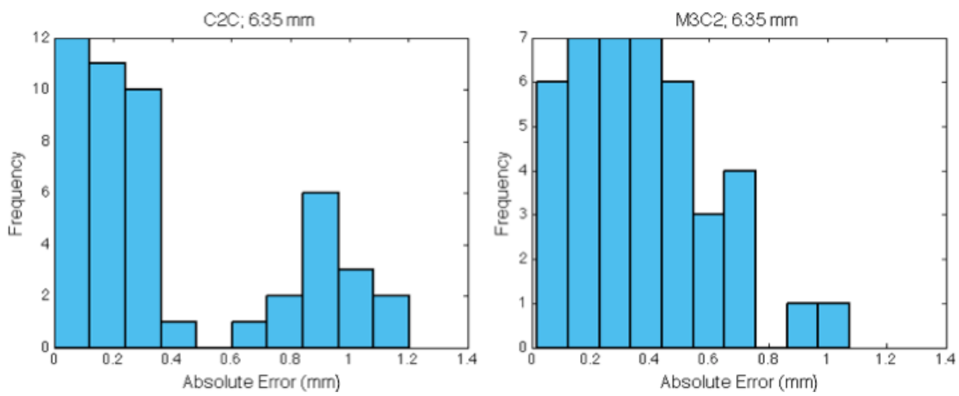

Figure 24. Absolute error distribution of 6.35 mm specimen

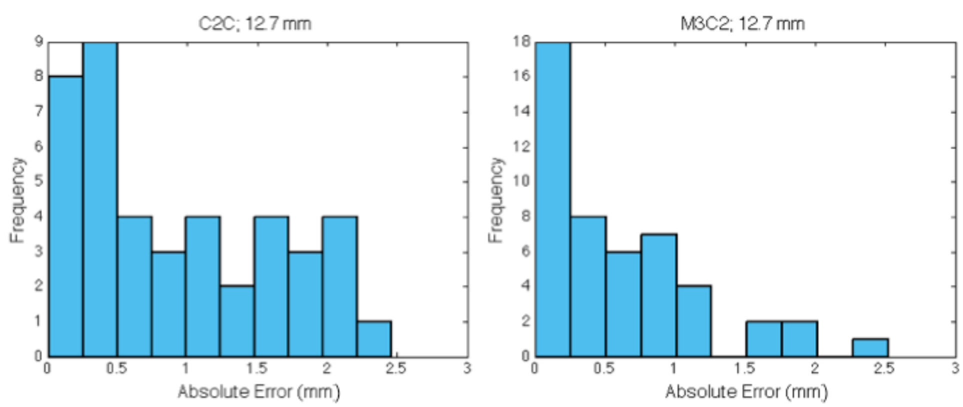

Figure 25. Absolute error distribution of 12.7 mm specimen

The absolute error histogram plot are all skewed right and most of the absolute errors are between 0 and 0.5 mm. M3C2 compared to C2C has a relatively lower number of absolute error larger than 1 mm. This indicates M3C2 was more accurate in measurement computation compared to C2C.

As an example, Figure 26 shows the C2C vs. M3C2 distance computation for the midspan deflection of 3.1 mm for the 6.35 mm specimen. As it seems, M3C2 has performed better in computing the deflections and is closer to the theoretical values.

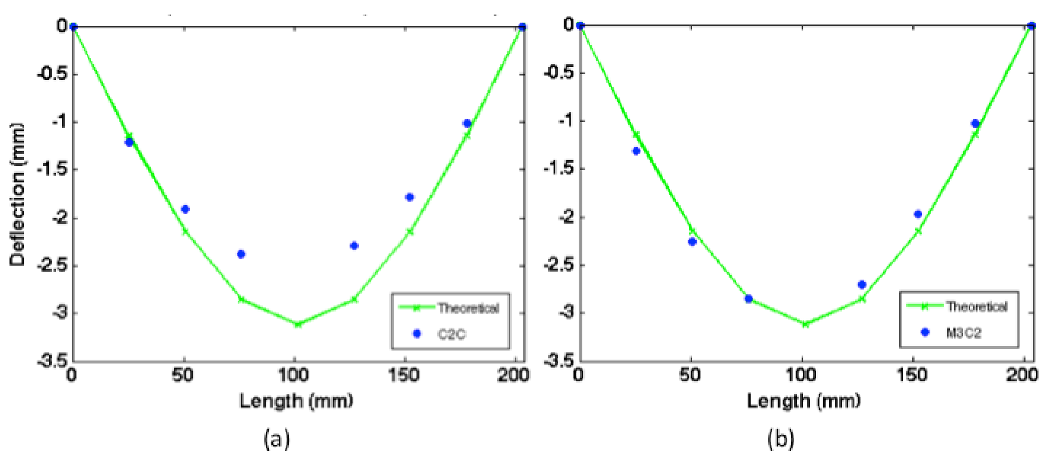

Figure 26. C2C vs. M3C2 deflection computation for the midspan deflection of 3.1 mm; 6.35 mm specimen; (a) C2C and (b) M3C2

Sources of Error:

The most significant source of error in the measurements is the misalignment of the two point clouds during the registration step. This step requires at least a partially manual registration, thus misalignment can result in spurious differences between the two clouds. Fine registration based on the ICP algorithm is sensitive to noise and an arbitrary initial state of the point clouds, and so implementing more advanced variants of the original ICP algorithm, such as assigning weightings to corresponding point pairs, or applying global deterministic optimizations or stochastic techniques would result in more reliable final registrations (Tam et al. 2013).

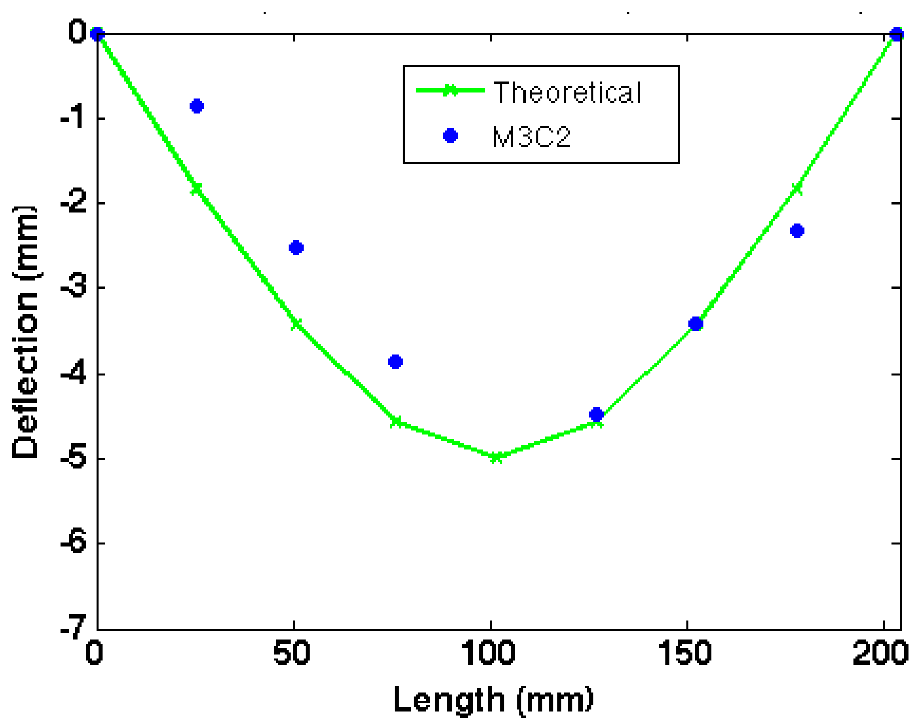

Figure 27. Registration error

For example in Figure 27, the calculated deflections on the left side are lower than the right side of the specimen. The reason is at registration step, the deflected point cloud was slightly rotated clockwise and caused this error. This error can be fixed manually by inspecting the registration step more closely.

Other sources of error include uncertainty in the mechanical properties of the specimen that affects the theoretical values, from the DSfM reconstruction process, as well as incorrect matching of points during nearest neighbors' computations. In addition, measuring distances using direct cloud-to-cloud comparison with closest point technique (Girardeau-Montaut et al. 2005b) is sensitive to the clouds' roughnesses, outliers, and point spacing which can lead to erroneous deformation calculations.

CHAPTER 5: CONCLUSIONS

This research introduces a new method of measuring structural deformation for monitoring purposes through direct point cloud comparison in 3D. Overall, the findings indicate that comparative point cloud analysis techniques are capable of highly accurate deformation measurements, with sub-millimeter accuracy. Additionally, it was found that the M3C2 algorithm performed better in comparison with C2C algorithm and the 10-point-sampling method with an absolute error of 0.4 mm. This degree of accuracy indicates the potential of this technique in remote sensing applications, in particular those where small deformations are of vital importance and where conventional sensor measurements are unavailable. This approach is feasible in scenarios where highly localized deformations have occurred, for instance in regions of local flange buckling, due to the high resolution per-point measurements enabled by this approach. Polynomial and curve fitting methods that fit points to a globally assumed shape are of limited benefit in such scenarios.

The biggest challenge was in the pre-processing stage, in particular, the alignment and registration. When the deflections are relatively small, for instance for the 12.7 mm specimen, the distance computations become very sensitive to registration errors. Therefore, more attention is required for the correct alignment and registration of the clouds.

These experiments were performed in a highly controlled laboratory environment. In order for this process to be successfully implemented for infrastructure evaluations, the robustness and accuracy of this measurement technique must be evaluated in field scenarios. Ongoing and future work seeks to improve the point sampling and measurement process and compare the results with cloud-to-mesh and mesh-to-mesh analysis. Moreover, the developed sampling technique can be used to update the structure's Finite Element Model (FEM) to account for deformations in the structure and conduct stress analyses.

APPENDIX

MATLAB Code:

Below is the MATLAB code used to sample the deflections and compare them with theoretical values. The input needs to be changed according to the specimen thickness and the recorded force from the UTM.

```
%% Bahman Jafari

clear;clc;close all

%% Theoretical

format long g

E=10000*1000;

b=1; h=.25;

I=(b*h^3)/12;

%% C2C

pct=95;

clmn=12; %column number in the text files

filename = '1l_8.txt';

M = dlmread(filename,'\t',2,0);

C2C = M(:,clmn);

Y = prctile(C2C,pct);

filename = '2l_8.txt';
```

```
M2 = dlmread(filename,'\t',1,0);

C2C2 = M2(:,clmn);

Y2 = prctile(C2C2,pct);

filename = '3l_8.txt';

M3 = dlmread(filename,'\t',1,0);

C2C3 = M3(:,clmn);

Y3 = prctile(C2C3,pct);

filename = '4l_8.txt';

M4 = dlmread(filename,'\t',1,0);

C2C4 = M4(:,clmn);

Y4 = prctile(C2C4,pct);

filename = '5l_8.txt';

M5 = dlmread(filename,'\t',1,0);

C2C5 = M5(:,clmn);

Y5 = prctile(C2C5,pct);

filename = '6l_8.txt';

M6 = dlmread(filename,'\t',1,0);

C2C6 = M6(:,clmn);

Y6 = prctile(C2C6,pct);

filename = '7l_8.txt';

M7 = dlmread(filename,'\t',1,0);

C2C7 = M7(:,clmn);
```

```
Y7 = prctile(C2C7,pct);
%% Plots
p=150;
xtp=[0 1 2 3 4 5 6 7 8];
xt2=[0 1 2 3 4];
yth2=-(p.*xt2)/(48*E*I).*(3*8^2-4*xt2.^2);
y_th=25.4*[yth2(1) yth2(2) yth2(3) yth2(4) yth2(5) yth2(4) yth2(3) yth2(2)
yth2(1)];
plot(25.4*xtp,y_th,'gx-')
hold on
x=(0:8);
y=-25.4*[0,Y,Y2,Y3, NaN, Y5,Y6,Y7,0];
dif=abs(y)-abs(y_th);
abs_dif=abs(dif);
scatter(25.4*x,y);
xlabel('Length (mm)','FontSize',16,'FontWeight','bold')
ylabel('Deflection (mm)','FontSize',16,'FontWeight','bold')
hold off
title('Thickness 6.35 mm, Deflection 3.106 mm, Percentile 95, Force 667 N',...
    'FontSize',16,'FontWeight','bold')
legend('Theoretical', 'C2C')
```

REFERENCES

Agisoft PhotoScan (version 0.9.1). 2013. Professional Edition. AgiSoft LLC. http://www.agisoft.com/.

Aiger, Dror, Niloy J. Mitra, and Daniel Cohen-Or. 2008. “4pointss Congruent Sets for Robust Pairwise Surface Registration.” In *ACM SIGGRAPH 2008 Papers*, 85:1–85:10. SIGGRAPH ’08. New York, NY, USA: ACM. doi:10.1145/1399504.1360684.

Baek, Dongyoub, Sungmin Cho, and Hyunwoo Bang. 2014. “Wheel Alignment Inspection by 3D Point Cloud Monitoring.” *Journal of Mechanical Science and Technology* 28 (4): 1465–71. doi:10.1007/s12206-014-0133-3.

Besl, Paul J., and Neil D. McKay. 1992. “Method for Registration of 3-D Shapes.” In , 1611:586–606. doi:10.1117/12.57955.

Bian, Haitao, Libin Bai, Shen-En Chen, and Sheng-Guo Wang. 2012. “Lidar Based Edge-Detection for Bridge Defect Identification.” In , 8347:83470X–83470X–10. San Diego, CA. doi:10.1117/12.915264.

Butt, M. Akmal, and P. Maragos. 1998. “Optimum Design of Chamfer Distance Transforms.” *IEEE Transactions on Image Processing* 7 (10): 1477–84. doi:10.1109/83.718487.

Cabaleiro, M., B. Riveiro, P. Arias, and J. C. Caamaño. 2015a. “Algorithm for Beam Deformation Modeling from LiDAR Data.” *Measurement*. http://www.sciencedirect.com/science/article/pii/S0263224115004364.

———. 2015b. “Algorithm for the Analysis of Deformations and Stresses due to Torsion in a Metal Beam from LIDAR Data.” *Structural Control and Health Monitoring*, January, n/a-n/a. doi:10.1002/stc.1824.

Cabaleiro, Manuel, Belén Riveiro, Pedro Arias, and José C. Caamaño. n.d. “Algorithm for the Analysis of the Geometric Properties of Cross-Sections of Timber Beams with Lack of Material from LIDAR Data.” *Materials and Structures*, 1–14.

Chen, B. Q., Y. Garbatov, and C. Guedes Soares. 2011. “Measurement of Weld-Induced Deformations in Three-Dimensional Structures Based on Photogrammetry Technique.” *Journal of Ship Production & Design* 27 (2): 51–62.

CloudCompare (version 2.6.1). n.d. http://www.danielgm.net/cc/.

Fathi, Habib, Fei Dai, and Manolis Lourakis. 2015. “Automated as-Built 3D Reconstruction of Civil Infrastructure Using Computer Vision: Achievements, Opportunities, and Challenges.” *Advanced Engineering Informatics* 29 (2): 149–67. doi:10.1016/j.aei.2015.01.012.

Fuchs, P., G. Washer, S. Chase, and M. Moore. 2004. “Applications of Laser-Based Instrumentation for Highway Bridges.” *Journal of Bridge Engineering* 9 (6): 541–49. doi:10.1061/(ASCE)1084-0702(2004)9:6(541).

Girardeau-Montaut, D., M. Roux, R. Marc, and G. Thibault. 2005a. “Change Detection on Points Cloud Data Acquired with a Ground Laser Scanner.” *International Archives of Photogrammetry, Remote Sensing and Spatial Information Sciences* 36 (part 3): W19.

———. 2005b. “Change Detection on Points Cloud Data Acquired with a Ground Laser Scanner.” *International Archives of Photogrammetry, Remote Sensing and Spatial Information Sciences* 36 (part 3): W19.

González-Aguilera, Diego, Ángel Muñoz-Nieto, Pablo Rodríguez-Gonzalvez, and Juan Mancera-Taboada. 2013. “Accuracy Assessment of Vehicles Surface Area Measurement by Means of Statistical Methods.” *Measurement* 46 (2): 1009–18. doi:10.1016/j.measurement.2012.04.021.

Hirschmuller, H. 2008. “Stereo Processing by Semiglobal Matching and Mutual Information.” *IEEE Transactions on Pattern Analysis and Machine Intelligence* 30 (2): 328–41. doi:10.1109/TPAMI.2007.1166.

Hossain, M. Julius, M. Ali Akber Dewan, Kiok Ahn, and Oksam Chae. 2011. “A Linear Time Algorithm of Computing Hausdorff Distance for Content-Based Image Analysis.” *Circuits, Systems, and Signal Processing* 31 (1): 389–99. doi:10.1007/s00034-011-9284-y.

Jafari, Bahman, Ali Khaloo, and David Lattanzi. 2016. “Long-Term Monitoring of Structures through Point Cloud Analysis.” In , 9805:98052K–98052K–8. doi:10.1117/12.2217586.

Jiang, Ruinian, and David V. Jauregui. 2010. “Development of a Digital Close-Range Photogrammetric Bridge Deflection Measurement System.” *Measurement* 43 (10): 1431–38. doi:10.1016/j.measurement.2010.08.015.

Khaloo, Ali, and David Lattanzi. 2015. “A Hierarchical Computer Vision Approach to Infrastructure Inspection.” In *Computing in Civil Engineering 2015*, 540–47. American Society of Civil Engineers. http://ascelibrary.org/doi/abs/10.1061/9780784479247.067.

Lague, Dimitri, Nicolas Brodu, and Jérôme Leroux. 2013. “Accurate 3D Comparison of Complex Topography with Terrestrial Laser Scanner: Application to the Rangitikei Canyon (N-Z).” *ISPRS Journal of Photogrammetry and Remote Sensing* 82 (August): 10–26. doi:10.1016/j.isprsjprs.2013.04.009.

Lattanzi, D., and G. Miller. 2015. “3D Scene Reconstruction for Robotic Bridge Inspection.” *Journal of Infrastructure Systems* 21 (2): 4014041. doi:10.1061/(ASCE)IS.1943-555X.0000229.

Li, Wen-long, Li-ping Zhou, and Si-Jie Yan. 2015. “A Case Study of Blade Inspection Based on Optical Scanning Method.” *International Journal of Production Research* 53 (7): 2165–78. doi:10.1080/00207543.2014.974851.

Liu, W., S. Chen, and E. Hasuer. 2012. “Bridge Clearance Evaluation Based on Terrestrial LIDAR Scan.” *Journal of Performance of Constructed Facilities* 26 (4): 469–77. doi:10.1061/(ASCE)CF.1943-5509.0000208.

Mouragnon, Etienne, Maxime Lhuillier, Michel Dhome, Fabien Dekeyser, and Patrick Sayd. 2009. “Generic and Real-Time Structure from Motion Using Local Bundle Adjustment.” *Image and Vision Computing* 27 (8): 1178–1193.

Pătrăucean, Viorica, Iro Armeni, Mohammad Nahangi, Jamie Yeung, Ioannis Brilakis, and Carl Haas. 2015. “State of Research in Automatic as-Built Modelling.” *Advanced Engineering Informatics*, Infrastructure Computer Vision, 29 (2): 162–71. doi:10.1016/j.aei.2015.01.001.

Rusu, Radu Bogdan, Zoltan Csaba Marton, Nico Blodow, Mihai Dolha, and Michael Beetz. 2008. “Towards 3D Point Cloud Based Object Maps for Household Environments.” *Robotics and Autonomous Systems*, Semantic Knowledge in Robotics, 56 (11): 927–41. doi:10.1016/j.robot.2008.08.005.

Seitz, S.M., B. Curless, J. Diebel, D. Scharstein, and R. Szeliski. 2006. “A Comparison and Evaluation of Multi-View Stereo Reconstruction Algorithms.” In *2006 IEEE Computer Society Conference on Computer Vision and Pattern Recognition*, 1:519–28. doi:10.1109/CVPR.2006.19.

Tam, G.K.L., Zhi-Quan Cheng, Yu-Kun Lai, F.C. Langbein, Yonghuai Liu, D. Marshall, R.R. Martin, Xian-Fang Sun, and P.L. Rosin. 2013. “Registration of 3D Point Clouds and Meshes: A Survey from Rigid to Nonrigid.” *IEEE Transactions on Visualization and Computer Graphics* 19 (7): 1199–1217. doi:10.1109/TVCG.2012.310.

Valença, J., D. Dias-da-Costa, E. Júlio, H. Araújo, and H. Costa. 2013. “Automatic Crack Monitoring Using Photogrammetry and Image Processing.” *Measurement* 46 (1): 433–41. doi:10.1016/j.measurement.2012.07.019.

Watson, Christopher, Shen-En Chen, Haitao Bian, and Edd Hauser. 2011. “3D Terrestrial Lidar for Operational Bridge Clearance Measurements.” In , 7983:79831M–79831M–14. San Diego, California, USA. doi:10.1117/12.880331.

Westoby, M. J., J. Brasington, N. F. Glasser, M. J. Hambrey, and J. M. Reynolds. 2012. “‘Structure-from-Motion’ Photogrammetry: A Low-Cost, Effective Tool for Geoscience Applications.” *Geomorphology* 179 (December): 300–314. doi:10.1016/j.geomorph.2012.08.021.

Yılmaztürk, F., S. Kulur, and N. Terzi. 2010. “Measurement of Deflections in Buried Flexible Pipes by Close Range Digital Photogrammetry.” *Measurement* 43 (6): 857–65. doi:10.1016/j.measurement.2010.03.005.

BIOGRAPHY

Bahman Moghaddame-Jafari graduated from Noor High School (Mashhad, Iran) in 2006. He received his Bachelor of Science in Civil Engineering from Islamic Azad University – Kashmar Branch in 2012. In the fall of 2014, he started his master's degree program at Volgenau School of Engineering at George Mason University (GMU). He was Teaching Assistant at the department of Civil, Environmental, and Infrastructure Engineering for three semesters. Moreover, he was part of Dr. Lattanzi research group at GMU where he worked on his master's thesis. In the summer of 2016, he was accepted in the Pathways Internship program with the United States Federal Government where he was a Civil Engineer at Federal Highway Administration headquarters in the Office of Infrastructure. Later that year in the fall of 2016, he graduated from GMU and received his Master of Science in Structural Engineering.